The Western Gulf of Corinth (Greece) 2020–2021 Seismic Crisis and Cascading Events: First Results from the Corinth Rift Laboratory Network

George Kaviris, Panagiotis Elias, Vasilis Kapetanidis, Anna Serpetsidaki, Andreas Karakonstantis, Vladimír Plicka, Louis de Barros, Efthimios Sokos, Ioannis Kassaras, Vassilis Sakkas, et al.

The Seismic Record
A journal of the Seismological Society of America

The Western Gulf of Corinth (Greece) 2020–2021 Seismic Crisis and Cascading Events: First Results from the Corinth Rift Laboratory Network

George Kaviris* *et al.*

Abstract

We investigate a seismic crisis that occurred in the western Gulf of Corinth (Greece) between December 2020 and February 2021. This area is the main focus of the Corinth Rift Laboratory (CRL) network, and has been closely monitored with local seismological and geodetic networks for 20 yr. The 2020–2021 seismic crisis evolved in three stages: It started with an M_w 4.6 event near the northern shore of the Gulf, opposite of Aigion, then migrated eastward toward Trizonia Island after an M_w 5.0 event, and eventually culminated with an M_w 5.3 event, ~3 km northeast of the Psathopyrgos fault. Aftershocks gradually migrated westward, triggering another cluster near the junction with the Rion–Patras fault. Moment tensor inversion revealed mainly normal faulting; however, some strike-slip mechanisms also exist, composing a complex tectonic regime in this region dominated by east–west normal faults. We employ seismic and geodetic observations to constrain the geometry and kinematics of the structures that hosted the major events. We discuss possible triggering mechanisms of the second and third stages of the sequence, including fluids migration and aseismic creep, and propose potential implications of the M_w 5.3 mainshock for the seismic hazard of the region.

Cite this article as Kaviris, G., Elias, P., Kapetanidis, V., Serpetsidaki, A., Karakonstantis, A., Plicka, V., De Barros, L., Sokos, E., Kassaras, I., Sakkas, V., *et al.* (2021). The Western Gulf of Corinth (Greece) 2020–2021 Seismic Crisis and Cascading Events: First Results from the Corinth Rift Laboratory Network, *The Seismic Record*. **1**, 85–95, doi: 10.1785/0320210021.

Supplemental Material

Introduction

The Corinth rift (central Greece) is a Quaternary graben characterized by ~east–west normal faulting. The western Gulf of Corinth (WGoC) is its most active region (Fig. 1), with an extension rate reaching 15 mm · yr^{-1} across N009°E (Briole *et al.*, 2021). Seismicity level is high (Makropoulos *et al.*, 2012), with the most recent $\mathbf{M} > 6$ event being the 1995 M_s 6.2 Aigion earthquake (Bernard *et al.*, 1997, Fig. 1). Since 2010, several events with $M_w \geq 5.0$ have occurred: the January 2010 M_w 5.2–5.3 Efpalio doublet (Sokos *et al.*, 2012), the November 2014 M_w 5.0 (Kaviris *et al.*, 2018), and the March 2019 M_w 5.1 earthquakes. Major active north-dipping structures include the Pirgaki, Helike, Aigion, and Psathopyrgos faults in the south, whereas the Marathias and Trizonia faults on the northern coast are south-dipping and steeper. The westward continuation of the Psathopyrgos fault turns to the Rion–Patras fault and runs inland north of Patras—the third-largest city in Greece. Farther south, the Rion–Patras fault runs offshore, likely connecting to the causative strike-slip fault of the 2008 Movri earthquake (Serpetsidaki *et al.*, 2014).

In the early 2000s, the Corinth Rift Laboratory network (CRLnet) was established, covering a 30 km × 30 km area in the WGoC (Cornet *et al.*, 2004). CRL is one of the Near-Fault Observatories (NFO) of the European Plate Observing System, and the only with an international status. It is administered and maintained by the Centre National de la Recherche Scientifique (France), the National and Kapodistrian University of Athens (NKUA-Greece), the University of

Full author list and affiliations appear at the end of this article.

*Corresponding author: gkaviris@geol.uoa.gr

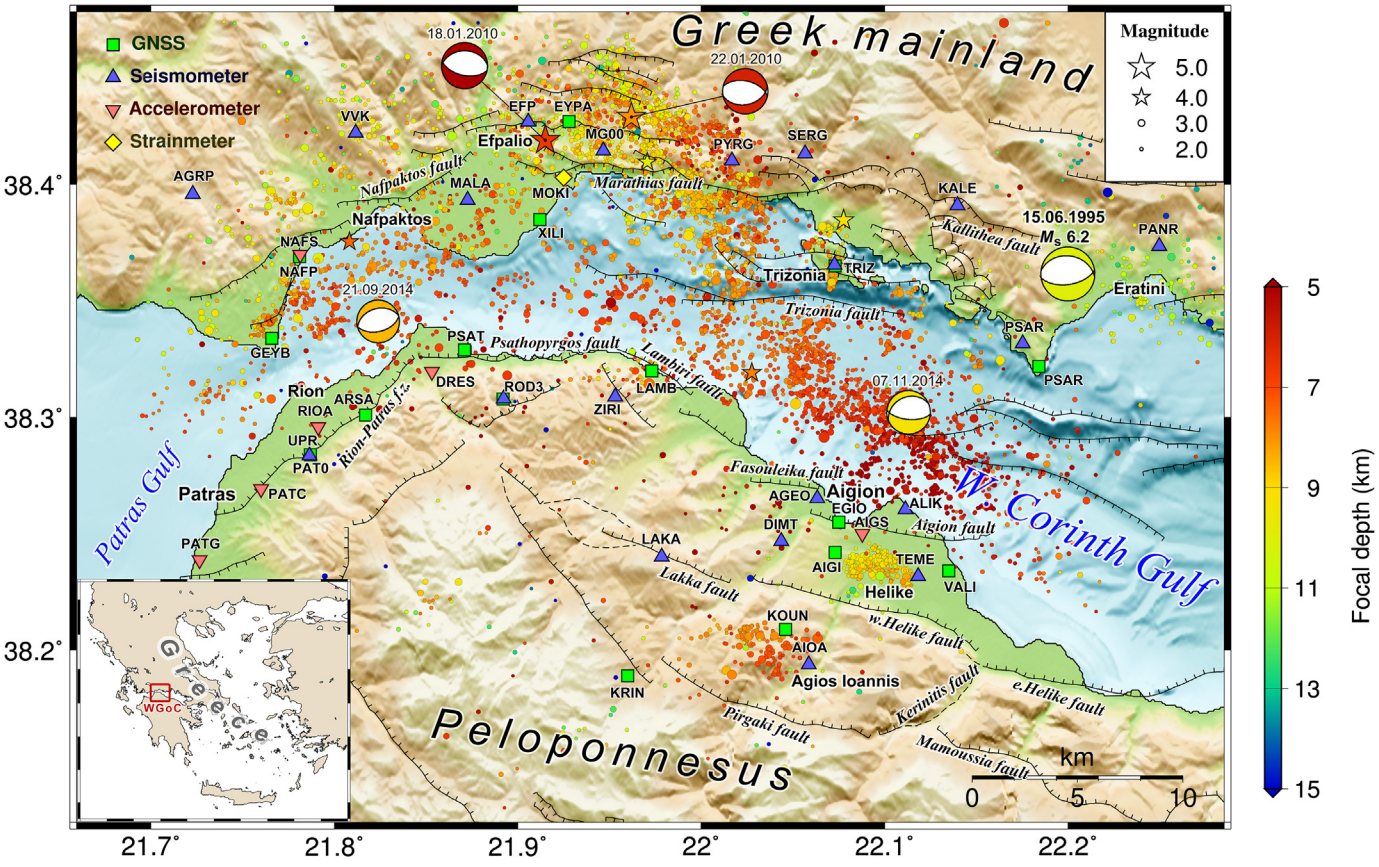

Figure 1. Seismotectonic map of the western Corinth rift. The epicenters of relocated seismicity ($M_w \geq 2.0$) during 2000–2015 are after Duverger *et al.* (2018) and are depicted as circles or stars (the latter for $M_w \geq 4.5$) with size proportional to magnitude. Focal mechanisms of events with $M_w \geq 5.0$ are displayed; the 15 June 1995 M_s 6.2 event is after Bernard *et al.* (1997); the 2010 Efpalio doublet is after Sokos *et al.* (2012); other focal mechanisms by Seismological Laboratory of National and Kapodistrian University of Athens (NKUA-SL). Seismological stations of the Corinth Rift Laboratory (CRL) network are depicted by blue upright (seismometers) and pink inverted (accelerometers) triangles; Global Navigation Satellite Systems (GNSS) stations are represented by green squares; the in Monastiraki (MOKI) strainmeter is marked with a yellow diamond. The location of the western Gulf of Corinth (WGoC) in central Greece is shown in the inset map. For fault lines, see Kapetanidis *et al.* (2015), Duverger *et al.* (2018), and references therein.

Patras (Greece), and the National Observatory of Athens (NOA-Greece), with the participation of Charles University (Czech Republic). NFOs are long-term observation and research infrastructures, tailored to provide high-resolution multidisciplinary data and products in the near field of faults of major importance in Europe. CRLnet comprises 80+ permanent stations, equipped with seismometers, accelerometers, Global Navigation Satellite Systems (GNSS), tide gauges, and strainmeters (Fig. 1). It enables detailed monitoring of the fluctuations of the intense microseismicity and deformation. The seismicity is clustered in time and space, with episodic seismic sequences, for example, the 2003–2004 offshore WGoC (Duverger *et al.*, 2015), 2013 Helike (Kapetanidis *et al.*, 2015; Mesimeri *et al.*, 2016), and 2015 Malamata (De Barros *et al.*, 2020) swarms. GNSS recordings and Interferometric Synthetic Aperture Radar (InSAR) revealed the deformation sources of moderate earthquakes and the likely existence of aseismic slip at shallow depth in some places (Elias and Briole, 2018).

On 23 December 2020, an intense seismic crisis started in the WGoC with an M_w 4.6 event at the northern coast, near Marathias. It was followed by several larger events. The sequence culminated with a 17 February 2021 M_w 5.3 event, north of the eastern edge of the Psathopyrgos fault. The westward expansion of the crisis raised concerns regarding potential impact on the densely populated urban area of Patras. The present study is a joint scientific effort of the CRL partners, aiming to characterize the structures activated during the sequence. We calculate hypocenters, focal mechanisms,

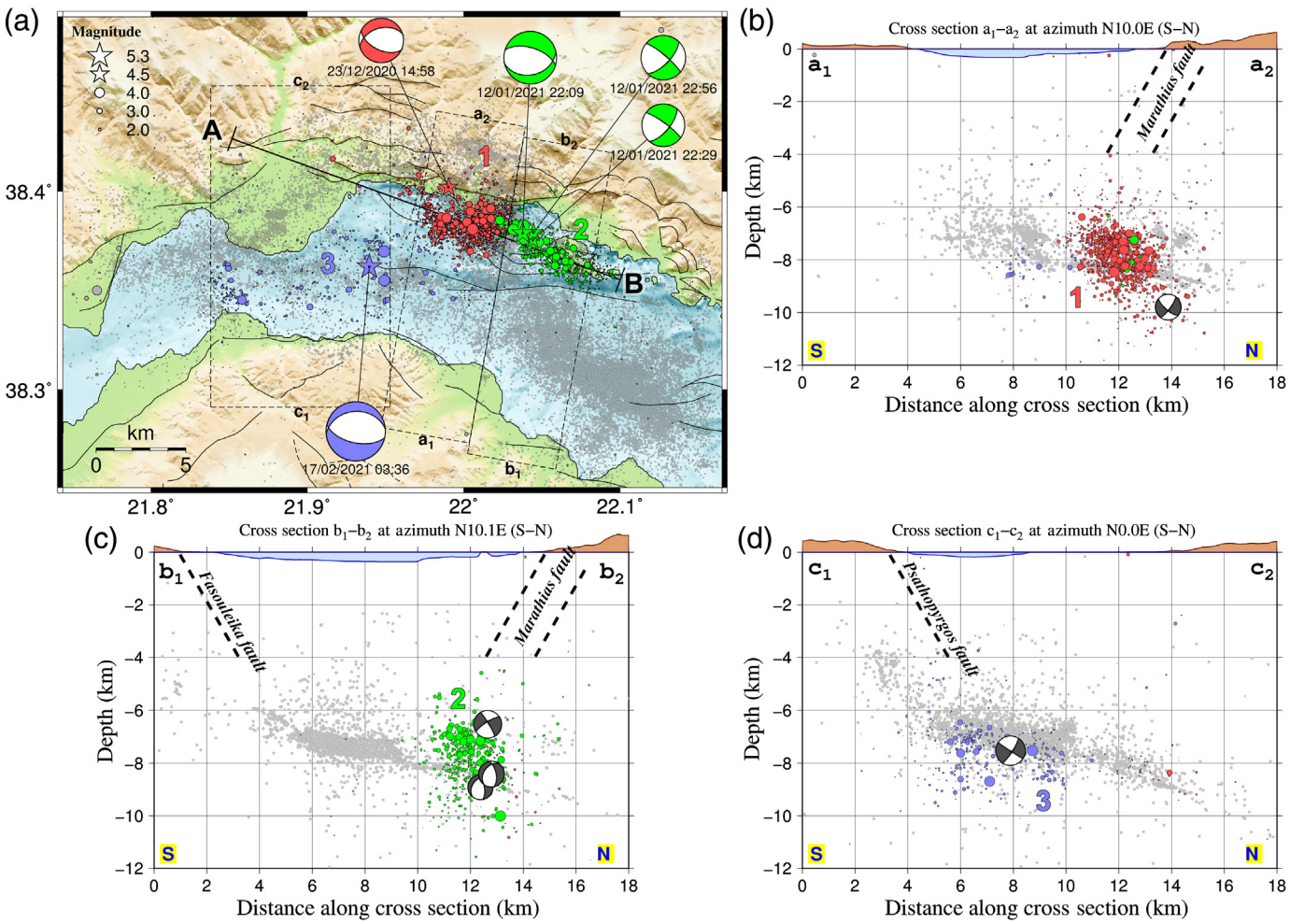

ground displacements at the GNSS stations, and Synthetic Aperture Radar (SAR) interferograms. We analyze the seismicity migration, and we discuss the role of the fluids and the possible existence of aseismic slip.

Figure 2. (a) Seismicity map for the period 23 December 2020–28 February 2021 divided into three spatial groups, indicated by different colors and numbers, with events of $M_w \geq 4.5$ represented by stars along with their respective focal mechanisms. Dashed rectangles mark the directions and boundaries of cross sections presented in panels (b–d). Dashed lines at the cross sections (b–d) are down-dip extensions of mapped faults, assuming an apparent dip angle of 60°. Light-gray dots indicate relocated seismicity of 2000–2015 (Duverger *et al.*, 2018).

Seismological Methods

We examined the seismicity recorded in the WGoC between 23 December 2020 and 28 February 2021. We analyzed 2960 events, with *P*- and *S*-wave arrival-time data manually determined at the Seismological Laboratory of NKUA and the Geodynamic Institute of NOA. Initial locations were assessed using HYPOINVERSE (Klein, 2002), tuning distance weighting by excluding stations located 40+ km away from the epicenters. We employed the 1D velocity model of Rigo *et al.* (1996); therefore, our locations are consistent with those of previous works using the same model (e.g., Duverger *et al.*, 2018). With a mean root mean square travel-time residual of 0.11 s, the average absolute location uncertainties reported by HYPOINVERSE are 0.31 km in horizontal and 0.86 km in vertical, supposing an average arrival-time reading error (i.e., picking measurement discrepancy from the true *P*- or *S*-wave arrival) of 0.13 s. For location uncertainties and other statistics, see Table S5 and Figures S3 and S4, available in the supplemental material to this article.

To facilitate the spatial and temporal description of the crisis, we divided the seismicity into three spatial groups, corresponding to the three main areas activated (Fig. 2). Cross sections in a roughly north–south direction (Fig. 2b–d) indicate that the

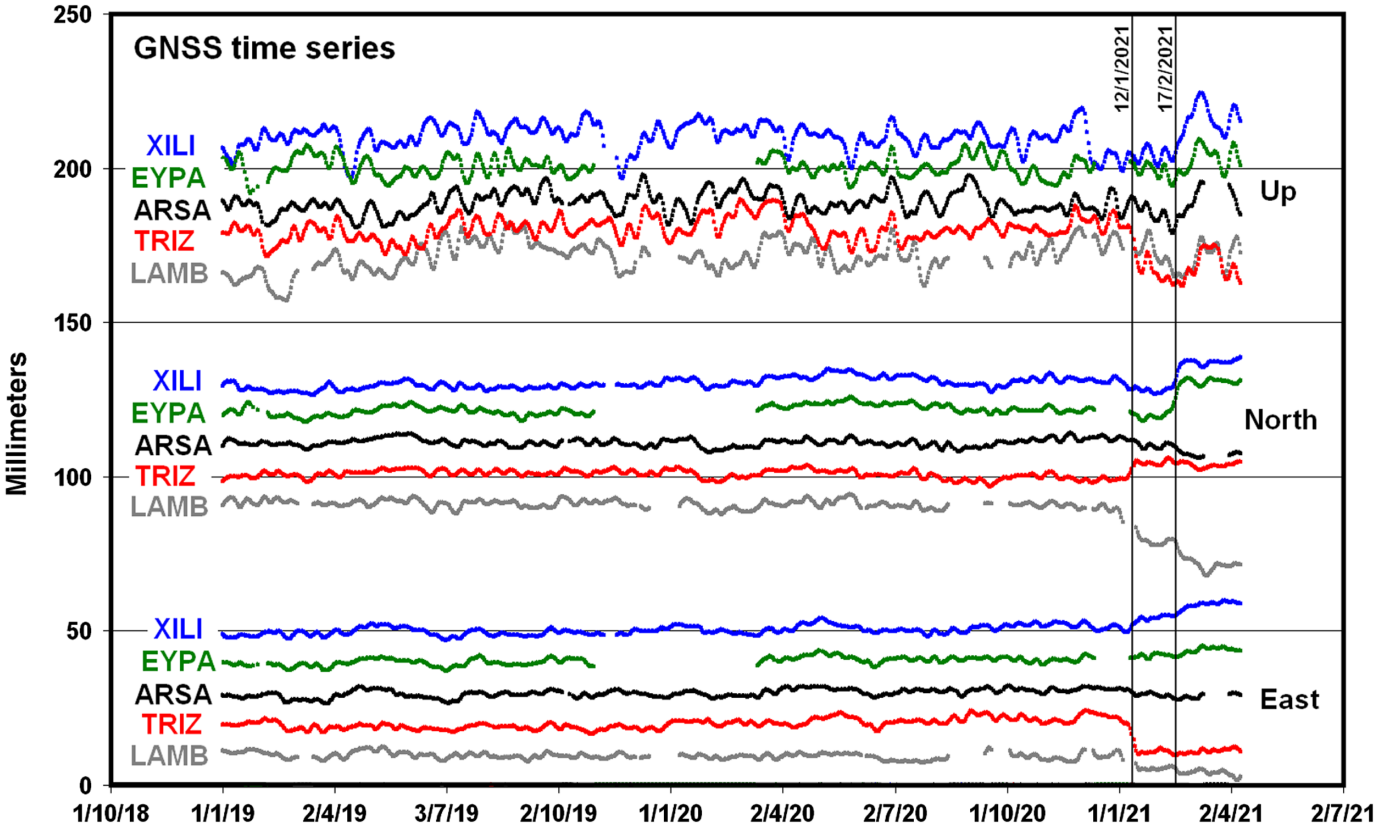

Figure 3. Displacement of the GNSS stations, including that induced by the earthquakes of 12 January and 17 February 2021.

hypocenters of groups 1 and 2 are located on north-dipping structures. The steeper group 2 shows a more linear distribution of its epicenters and includes strike-slip events. The sparser group 3 shows activity on a low-angle structure.

We calculated focal mechanisms through moment tensor inversion for the five strongest events (magnitudes between 4.5 and 5.3) using ISOLA software (Sokos and Zahradnik, 2008; Zahradník and Sokos, 2018) and the velocity model of Rigo *et al.* (1996). We used stations from both CRLnet and the Hellenic Unified Seismological Network, at a maximum epicentral distance of 60 km. Details on moment tensor inversion are available in the Moment Tensor Inversion Additional Information section in the supplemental material.

Geodetic Methods

GNSS data were processed using software GIPSY (version 6.4), developed by Jet Propulsion Laboratory–National Aeronautics and Space Administration. Following Briole *et al.* (2021), the time series were corrected for the secular velocities and filtered with a Gaussian filter. The residual time series are plotted in Figure 3, and the coseismic displacements are listed in Table S2. For the two main events (12 January 2021 M_w 5.0 and 17 February 2021 M_w 5.3), Sentinel-1 SAR interferometry (InSAR) shows no deformation within a quarter of fringe (7 mm) in the line-of-sight direction. Indicatively, an interferogram of Sentinel-1 Track 80, spanning the dates 12 and 24 January 2021, is shown in Figure S5.

Modeling was performed with Inverse6 code (Briole, 2017), using the method described by Briole *et al.* (1987). For both the events, we assumed a north-dipping fault plane with focal mechanisms given in Table S1. Along-shore displacement was constrained to be consistent with InSAR within ±7 mm. We inverted for the size, horizontal position, and depth of the rupture. The best-fitting solutions are listed in Table S3. The geodetic moment of the 12 January 2021 event (Table S3) is ~5 times larger than the one determined by seismology (Table S1), suggesting that prevailing transient aseismic slip dominated during that event.

Spatiotemporal evolution of the sequence

Certain major characteristics of the sequence are visualized through the projection of the epicenters along a N110°E-oriented

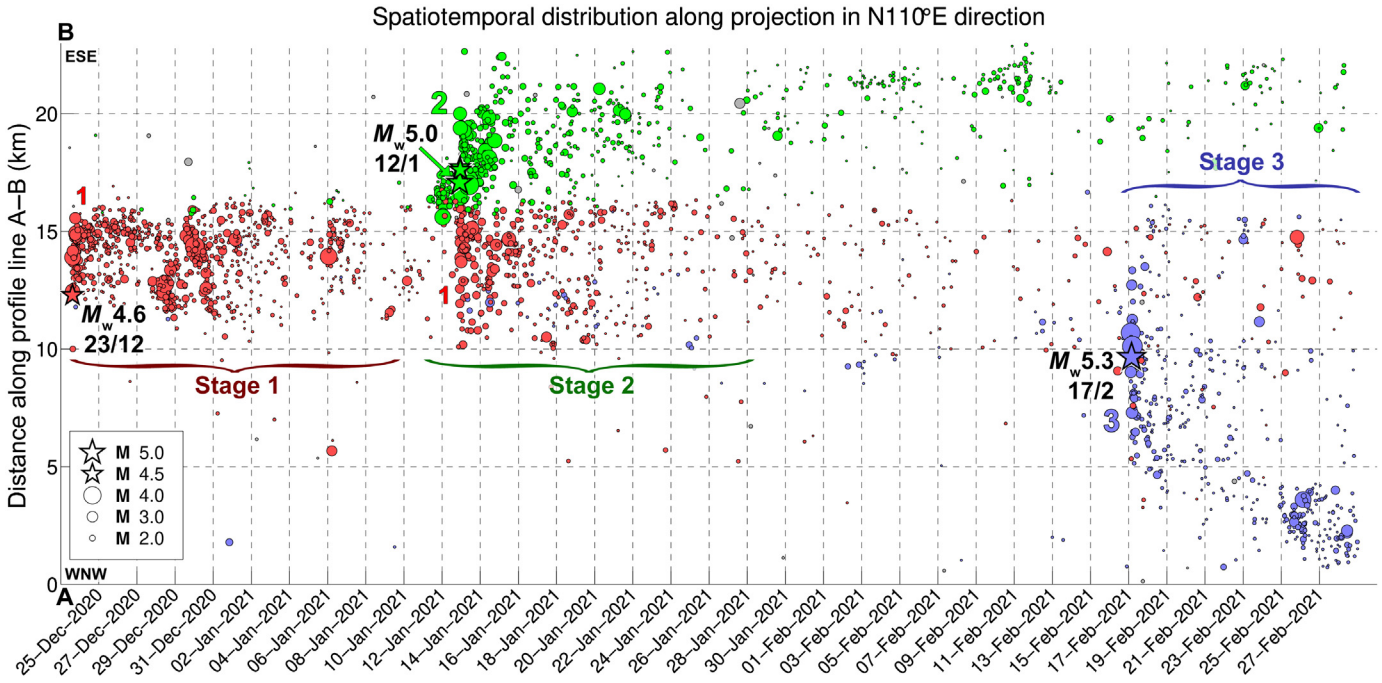

Figure 4. Spatiotemporal projection along the A–B profile depicted in Figure 2a for the period 23 December 2020–28 February 2021 (horizontal temporal axis). Colors and numbers represent the three spatial groups of Figure 2. Epicenters are depicted as circles or stars (the latter for $M_w \geq 4.5$) with size proportional to the magnitude. Three temporal stages and their main events are marked.

profile (line A–B of Fig. 2a) with respect to their origin time (Fig. 4). Three distinct stages are identified, marked by brackets. The first stage near Marathias, involving spatial group 1 (red), begins with the 23 December 2020 M_w 4.6 event and continues with aftershocks migrating mainly eastward on a 5 km long structure. The second stage starts with a short foreshock activity in group 2 (green), approximately two days before the 12 January 2021 M_w 5.0 event near Trizonia Island. This major event triggers seismicity that migrates both eastward and westward on a 12 km long alignment, penetrating the area of the previously active group 1. The third stage starts with the 17 February 2021 M_w 5.3 event in group 3 (blue). Its seismicity is located offshore, north of the Psathopyrgos fault. It migrates mainly westward and triggers a small cluster near the junction between the Psathopyrgos fault and the Rion–Patras fault zone. Overall, in the three month period, the crisis spans more than 20 km in an east–west direction. The speeds of seismic migration range from few hundreds of m/day to several km/day, in most cases spreading over distances of a few kilometers. The faster speeds are more likely driven by either afterslip in response to aftershocks, or slow slip when no mainshock exists, rather than by fluid diffusion, as previously observed in the WGoC (e.g., De Barros *et al.*, 2020).

Discussion

Our locations show that the December 2020–February 2021 seismic crisis activated several parts of a large-scale seismic layer, already identified by CRL since 2000. The latter is a volume (outlined in orange in Fig. 5) interpreted as a brittle, highly fractured, 1–3 km thick geological layer, between 6 and 9 km depth, gently dipping north, in which the main normal faults of the WGoC are rooting (Lambotte *et al.*, 2014; Duverger *et al.*, 2018).

Cluster 1 occurs in an area activated at least once a year since 2000 (except in 2003 and 2005) by similar swarms, with several events larger than **M** 4.0. The bulk of its activity spans from 7 to 9 km depth, consistent with the background seismicity, plotted for 2000–2015 in gray in Figures 2 and 5 (see also profiles 9–11 in Duverger *et al.*, 2018). The 2020–2021 sequence starts at the deep southeastern edge of the 2010 $M_w > 5$ doublet sequence (Sokos *et al.*, 2012), with the 23 December 2020 mainshock, which is located less than 2 km north of the 25 April 2012 M_w 4.3 earthquake, yet with a slightly different focal mechanism. The east–west-striking normal-fault mechanism of the 23 December 2020 mainshock fits the local stress field, associated with north–south extension (e.g., Kassaras *et al.*, 2016).

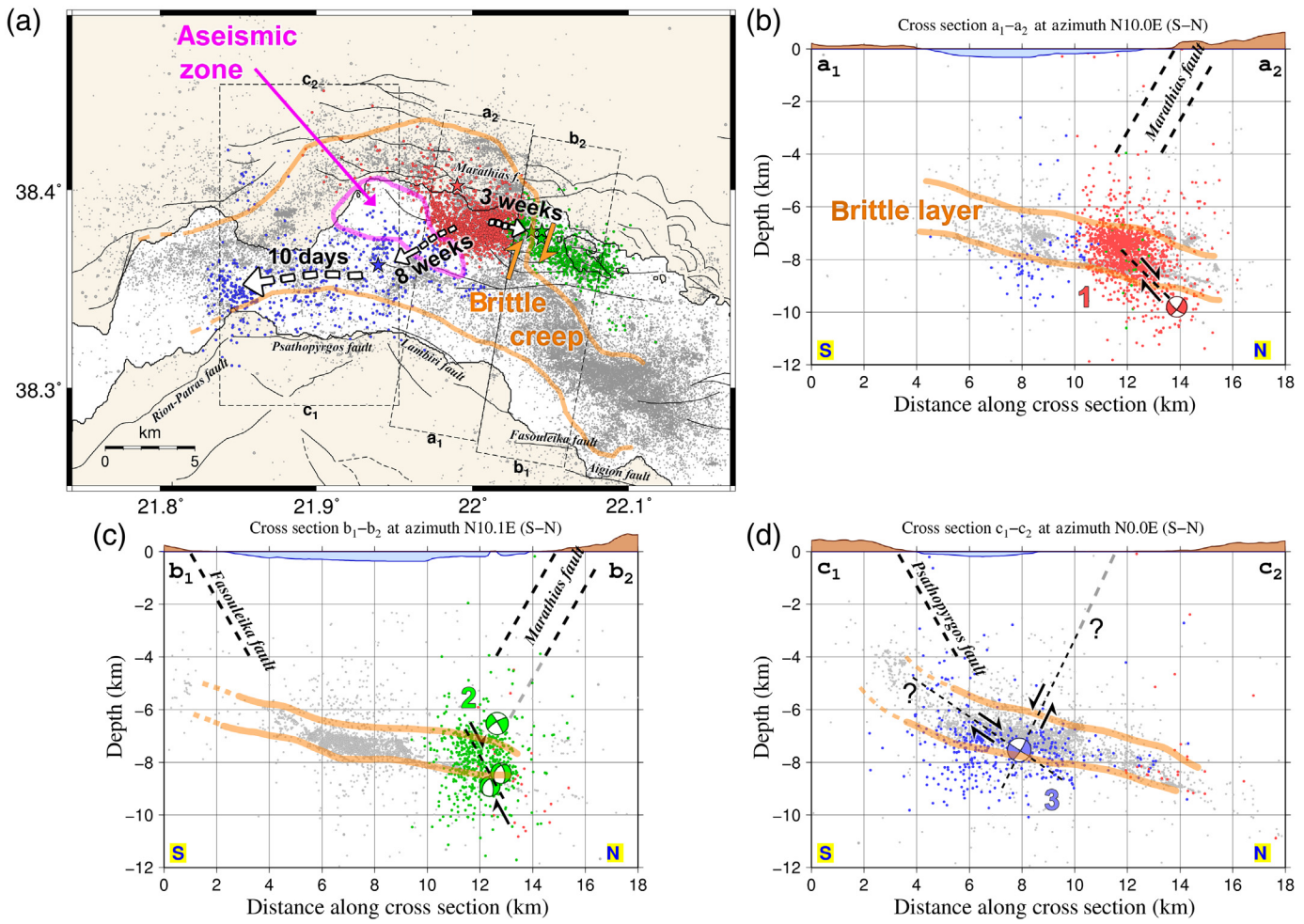

Figure 5. Interpretation sketch in (a) map and (b–d) cross sections, following the layout of Figure 2. The brittle layer is marked with orange lines, delineating the two dominant west–northwest to east–southeast-trending microseismic bands (one near Marathias and another south of Trizonia Island), connected by a north–south-trending band, proposed to be a broad right-lateral shear zone (orange half-arrows west of Trizonia). An aseismic zone between groups 1 and 3 is delimited in purple on the map. Proposed faults and their kinematics are marked with dashed lines and half-arrow pairs. Light-gray dots indicate relocated seismicity of 2000–2015 (Duverger *et al.*, 2018).

However, we could not resolve unambiguously the activated nodal plane.

The north-dipping solution requires a blind fault patch, necessarily small, as there is no evidence of such fault in the bathymetry at the expected outcropping position. This fault could connect to the active cluster up-dip. In this case, the seismic gap of 1.5 km between the mainshock focus and the microseismic cluster might reveal the extension of the main rupture (Fig. 5b).

The south-dipping solution would involve the Marathias fault system, outcropping a few kilometers north of the northern shoreline. This hypothesis is less likely, as the prolongation of the Marathias fault, at an assumed dip angle of 60°, misses the mainshock hypocenter by 4 km at the focal depth of 10 km, the latter value being supported by both hypocentral location and moment tensor centroid (Table S1). However, it directly intersects cluster 1, suggesting it may play an important role in activating it.

Cluster 2 starts with a three week delay at the eastern edge of cluster 1 (Fig. 4), with a two day foreshock sequence prior to the 12 January 2021 M_w 5.0 mainshock. The most likely fault plane is dipping north, owing to the shape of the western seismic cluster and to the expected several kilometers of the rupture (Fig. 5c). It involves an area where the seismic activity in the past 20 yr is much weaker than in the cluster 1 area. A few kilometers eastward, the east–west-striking normal-fault

mainshock triggers a sequence of moderate-magnitude strike-slip events. Similar events, with dextral mechanism on the north-northeast-striking nodal plane, have been previously reported in the same area (e.g., Rigo *et al.*, 1996; Godano *et al.*, 2014; Serpetsidaki *et al.*, 2016). Consistently, structurally controlled northeast–southwest mean anisotropy directions are inferred from the data of the nearby stations PYRG and SERG (Kaviris *et al.*, 2017, 2018).

During the past decade, evidence of a variety of mechanical responses to the stress field across the Corinth rift has grown (Sokos *et al.*, 2012; Valkaniotis and Pavlides, 2016; Sakellariou and Tsampouraki-Kraounaki, 2019). The predominant extension, expressed by the ∼east–west normal focal mechanisms, is accompanied by strike-slip faulting on localized transtensional features. The moderate events of cluster 2 occur at the northern tip of the north–south-distributed main microseismic band, plotted with gray dots in Figure 2 (and fig. 3 of Duverger *et al.*, 2018). This north–south active band (marked with orange arrows in Fig. 5) connects the two dominant microseismic groups—one located to the southeast (mid-gulf, south of Trizonia, and cluster 2) and the other to the northwest (near Marathias, northwest of cluster 1), both trending west-northwest to east-southeast and are subjected to dominant normal faulting (see orange line in Fig. 5a). The north–south band could constitute a broad right-lateral shear zone within the seismic layer. This would fit with the north–south offset between the Aigion–Fasouleika and Psathopyrgos normal-fault systems.

Located just east of the strike-slip epicenters, the structure reported in profiles P7 and P8 of Duverger *et al.* (2018) shows well-resolved thin active fault planes and long-term repeaters, diagnostic of their dominant creep. This is consistent with the easternmost activity of cluster 2 depicted in Figure 4 (close to point B), with a persistence of seismic bursts until late February 2021, contrasting with the fast activity decay more to the west, near the mainshock.

Eight weeks after the initiation of cluster 1, cluster 3 starts on 17 February 2021, with three cascading, moderate earthquakes, the largest being an M_w 5.3 event. The in-between area is only slightly activated at the outset of cluster 2, presumably as a response to the 12 January 2021 mainshock. Since 2000, it has been an area (purple zone in Fig. 5a) depleted of swarm activity, with only a few events with $\mathbf{M} > 3.0$ (and ≤3.5). This microseismic gap might be related to the geometry and rheology of the brittle crust, and to the kinematics and geometry of the normal faults that root into it. It might also correspond to a less fractured and less permeable part of the crust. Its origin and mechanical significance require further investigation.

Cluster 3 displays three subareas. The broad central part, coinciding with most of the east–west span of the Psathopyrgos fault, exhibits low-level, diffuse seismicity. Contrariwise, there are two narrow, active regions on both sides, with the triggering mainshocks to the east and a large persistent swarm to the west (Fig. 5a). The partitioning of this area has been recurrently observed during the past 20 yr, with swarms rarely spreading from one subarea to another. This stable pattern suggests a strong structural control of the extensional dynamics, presumably related to the northern continuation of the contact zone between the Psathopyrgos and the adjacent faults: the Rion–Patras fault to the west (see also Duverger *et al.*, 2018) and the Lambiri fault to the east. The ∼east–west-striking mechanism of the 17 February 2021 M_w 5.3 event is not related to the Lambiri fault, but rather to the easternmost part of the Psathopyrgos fault or an unknown antithetic fault segment. It has a rupture length of ∼5 km, constrained by GNSS data modeling, and is consistent with estimates of source duration (2.0–2.5 s from preliminary source inversion and corner frequencies from nearby accelerometers). Its size and location make the north-dipping nodal plane more likely to be the fault plane, as it better fits the rest of the microseismic volume, distributed in a northward-dipping layer (Fig. 5d). Notably, inversion of GNSS data implies a very shallow fault, with a centroid depth of 2.6 km. This is compatible with the centroid depth of 3.5 km yielded from seismological data (Table S1), but not with the hypocentral distribution. Deeper solutions lead to horizontal displacements inconsistent with the GNSS observations and much larger residuals (Table S4). It is possible that the rupture nucleated near 7.6 km (hypocentral depth), but then most slip occurred along a shallower part of the fault.

The sequence of clusters mixes dominant foreshock–mainshock–aftershock patterns prolonged with swarm-like trailing activity and internal microseismicity migration patterns. These minor diffusion episodes appear within the three clusters (see Fig. 4), on 27 and 28 December 2020 for cluster 1, on 12–16 January 2021 for cluster 2, and on 17–27 February 2021 for cluster 3, with migration rates of 1.5, 2.5, and 0.5 km/day, respectively. For clusters 1 and 2, the high velocities suggest a dominant transfer of stress through creep, assisted by the long-range effect of the largest coseismic ruptures. For cluster 3, the lower velocities fit with pore-pressure diffusion in a highly permeable layer, possibly assisted by creep. These values contrast with the slow migration speeds (10^{-3}–10^{-1} km/day),

previously observed in the central and the southern part of the rift and interpreted as pore-pressure diffusion in the fractured, seismogenic geological layer (Bourouis and Cornet, 2009; Lambotte *et al.*, 2014; Duverger *et al.*, 2015, 2018). For cluster 3, along the Psathopyrgos fault, the 0.5 km/day speed is close to the 0.3 km/day determined by Duverger *et al.* (2018) for the first seismic migration across the same area, in August–September 2014. Interestingly, the migration was eastward in 2014 and westward in 2021. This may be explained by the eastward boost of the initial slow slip in 2014 and the westward boost of the 2021 M_w 5.3 event, both acting on a similarly prestressed seismic layer, but in opposite directions. The lack of large-scale InSAR deformation for the entire 2020–2021 crisis and the weak GNSS signals near the origin time of the mainshocks show that, if any aseismic strain accompanied these mainshocks due to the inferred creep or to pore-pressure transients, the cumulative aseismic moment should not exceed that of the coseismic one, that is, $M_o \approx 2.02 \times 10^{17}$ N × m.

Conclusions and Perspectives

The 2020–2021 seismic crisis involved known active crustal structures of the WGoC, mixing dominant foreshock–mainshock–aftershock patterns with swarm-like activity. We document the migrations of seismicity and interpret them by creep and pore-pressure diffusion processes. The space–time clustering of the activity reflects the segmentation of the medium at the root of the major outcropping normal faults (i.e., Marathias and Psathopyrgos), possibly activating them or their antithetic fault systems.

The last phase of the sequence, near the Psathopyrgos fault, may have increased the probability of a large earthquake, either by coulomb stress changes or by dynamic weakening of the fault induced by the strong shaking of the nearby $\mathbf{M} > 5.0$ events. A possible dynamic rupture cascading westward on the Rion–Patras fault may further increase seismic hazard for the city of Patras. More work is needed to decipher this seismic sequence, and evaluate the impact on the surrounding major faults and the overall seismic hazard in the area.

Our study highlights the need of dense, continuous monitoring of the active faults, especially those being close to populated cities. Each seismic crisis captured by the CRLnet arrays provides new opportunities to refine the knowledge of the faults geometry, crustal structure, and rheology of the WGoC. The data and models allow to gradually gain insight into the fluid-related processes in the crust of the WGoC, which include pore-pressure diffusion, slow slip, and probably nonelastic deformation processes.

Data and Resources

Corinth Rift Laboratory network (CRLnet) comprises seismological, geodetic and geophysical subnetworks from various educational and research entities. The first instruments were installed in 2000. Seismological data were acquired with 20 broadband and short-period velocimeters and six accelerometers installed and operated by the following institutions: (1) the Corinth Rift Laboratory (CRL) team (CL network, data hosted at RESIF, DOI: 10.15778/RESIF.CL), (2) the National and Kapodistrian University of Athens (NKUA; HA network, DOI: 10.7914/SN/HA), (3) the University of Patras (HP network, DOI: 10.7914/SN/HP), which operates certain stations jointly with Charles University, Prague, and (4) the National Observatory of Athens (NOA; HL network, DOI: 10.7914/SN/HL) (Fig. 1). Stations by the last three institutes are also part of Hellenic Unified Seismological Network (HUSN). Global Navigation Satellite Systems (GNSS) observations were made with 13 stations (installed since 2002)—12 operated by the CRL team and one by Geodynamic Institute of NOA (GI-NOA). A three-component strainmeter (in Monastiraki [MOKI]) was installed by the CRL team in 2006, with a 3 m long sensing unit (Fig. 1). The supplemental material for this article includes Section S1: Moment tensor inversion additional information and Section S2: Additional tables and figures.

Data Availability Statement and Declaration

Data from seismometers and accelerometers can be retrieved from European Plate Observing System (EPOS) nodes (https://www.orfeus-eu.org/data/eida/nodes/), European Integrated Data Archive (EIDA) nodes at RESIF, and National Observatory of Athens (NOA; Evangelidis *et al.*, 2021). Global Navigation Satellite Systems (GNSS) data and positioning solutions are available on the Corinth Rift Laboratory (CRL) portal (http://crlab.eu). Phase and focal mechanism data of Seismological Laboratory of National and Kapodistrian University of Athens (NKUA-SL) are available at http://www.geophysics.geol.uoa.gr/stations/gmapv3_db/index.php?lang=en and of GI-NOA at http://bbnet.gein.noa.gr/HL/databases/database. The focal mechanism of the 25 April 2012 event is available at https://www.emsc-csem.org/Earthquake/tensors.php?id=263856&year=2012;UPSL. All websites were last accessed in July 2021.

Declaration of Competing Interests

The authors declare no competing interests.

Acknowledgments

The authors thank the personnel of Corinth Rift Laboratory network (CRLnet) and Hellenic Unified Seismological Network (HUSN) who worked for the installation, operation, and maintenance of stations used in this article. George Kaviris, Vasilis Kapetanidis, Anna Serpetsidaki, Andreas Karakonstantis, Efthimios Sokos, Ioannis Kassaras, Vassilis Sakkas, Ioannis Spingos, Christos Evangelidis, Ioannis Fountoulakis, Olga-Joan Ktenidou, Panayotis Papadimitriou, and Nicholas Voulgaris acknowledge financial support by the HELPOS project, "Hellenic Plate Observing System" (MIS 5002697). Maps and cross sections were drawn using the Generic Mapping Tools (GMT) software (Wessel and Smith, 1998).

References

Bernard, P., P. Briole, B. Meyer, J. Gomez, C. Tiberi, C. Berge, R. Cattin, D. Hatzfeld, C. Lachet, B. Lebrun, *et al.* (1997). The $M_s = 6.2$, June 15, 1995 Aigion earthquake (Greece): Evidence for low-angle normal faulting in the Corinth rift, *J. Seismol.* **1,** 131–150, doi: 10.1023/A:1009795618839.

Bourouis, S., and F. H. Cornet (2009). Microseismic activity and fluid fault interactions: Some results from the Corinth Rift Laboratory (CRL), Greece, *Geophys. J. Int.* **178,** 561–580, doi: 10.1111/j.1365-246X.2009.04148.x.

Briole, P. (2017). Modelling of earthquake slip by inversion of GPS and InSAR data assuming homogenous elastic medium, doi: 10.5281/ZENODO.1098399.

Briole, P., A. Ganas, P. Elias, and D. Dimitrov (2021). The GPS velocity field of the Aegean. New observations, contribution of the earthquakes, crustal blocks model, *Geophys. J. Int.* **226,** 468–492, doi: 10.1093/gji/ggab089.

Briole, P., R. Gaulon, G. De Natale, F. Pingue, and R. Scarpa (1987). Inversion of geodetic data and seismicity associated with the Friuli earthquake sequence (1976–1977), *Ann. Geophys.* **4,** no. B4, 481–492.

Cornet, F. H., P. Bernard, and I. Moretti (2004). The Corinth Rift Laboratory, *Compt. Rendus Geosci.* **336,** nos. 4/5, 235–241, doi: 10.1016/j.crte.2004.02.001.

De Barros, L., F. Cappa, A. Deschamps, and P. Dublanchet (2020). Imbricated aseismic slip and fluid diffusion drive a seismic swarm in the Corinth Gulf, Greece, *Geophys. Res. Lett.* **47,** no. 9, e2020GL087142, doi: 10.1029/2020GL087142.

Duverger, C., M. Godano, P. Bernard, H. Lyon-Caen, and S. Lambotte (2015). The 2003–2004 seismic swarm in the western Corinth rift: Evidence for a multiscale pore pressure diffusion process along a permeable fault system, *Geophys. Res. Lett.* **42,** 7374–7382, doi: 10.1002/2015GL065298.

Duverger, C., S. Lambotte, P. Bernard, H. Lyon-Caen, A. Deschamps, and A. Nercessian (2018). Dynamics of microseismicity and its relationship with the active structures in the western Corinth rift (Greece), *Geophys. J. Int.* **215,** 196–221, doi: 10.1093/gji/ggy264.

Elias, P., and P. Briole (2018). Ground deformations in the Corinth rift, Greece, investigated through the means of SAR multitemporal interferometry, *Geochem. Geophys. Geosys.* **19,** 4836–4857, doi: 10.1029/2018GC007574.

Evangelidis, C. P., N. Triantafyllis, M. Samios, K. Boukouras, K. Kontakos, O.-J. Ktenidou, I. Fountoulakis, I. Kalogeras, N. S. Melis, O. Galanis, *et al.* (2021). Seismic waveform data from Greece and Cyprus: Integration, archival, and open access, *Seismol. Res. Lett.* **92,** no. 3, 1672–1684, doi: 10.1785/0220200408.

Godano, M., A. Deschamps, S. Lambotte, H. Lyon-Caen, P. Bernard, and F. Pacchiani (2014). Focal mechanisms of earthquake multiplets in the western part of the Corinth rift (Greece): Influence of the velocity model and constraints on the geometry of the active faults, *Geophys. J. Int.* **197,** 1660–1680, doi: 10.1093/gji/ggu059.

Kapetanidis, V., A. Deschamps, P. Papadimitriou, E. Matrullo, A. Karakonstantis, G. Bozionelos, G. Kaviris, A. Serpetsidaki, H. Lyon-Caen, N. Voulgaris, *et al.* (2015). The 2013 earthquake swarm in Helike, Greece: Seismic activity at the root of old normal faults, *Geophys. J. Int.* **202,** 2044–2073, doi: 10.1093/gji/ggv249.

Kassaras, I., V. Kapetanidis, and A. Karakonstantis (2016). On the spatial distribution of seismicity and the 3D tectonic stress field in western Greece, *Phys. Chem. Earth* **95,** 50–72, doi: 10.1016/j.pce.2016.03.012.

Kaviris, G., C. Millas, I. Spingos, V. Kapetanidis, I. Fountoulakis, P. Papadimitriou, N. Voulgaris, and K. Makropoulos (2018). Observations of shear-wave splitting parameters in the western Gulf of Corinth focusing on the 2014 $M_w = 5.0$ earthquake, *Phys. Earth Planet. In.* **282,** 60–76, doi: 10.1016/j.pepi.2018.07.005.

Kaviris, G., I. Spingos, V. Kapetanidis, P. Papadimitriou, N. Voulgaris, and K. Makropoulos (2017). Upper crust seismic anisotropy study and temporal variations of shear-wave splitting parameters in the western Gulf of Corinth (Greece) during 2013, *Phys. Earth Planet. In.* **269,** 148–164, doi: 10.1016/j.pepi.2017.06.006.

Klein, F. W. (2002). User's guide to HYPOINVERSE-2000, a Fortran program to solve for earthquake locations and magnitudes, *U.S. Geol. Surv. Open-File Rept. 02-171*, 123 pp., available at http://geopubs.wr.usgs.gov/open-file/of02-171/ (last accessed July 2021).

Lambotte, S., H. Lyon-Caen, P. Bernard, A. Deschamps, G. Patau, A. Nercessian, F. Pacchiani, S. Bourouis, M. Drilleau, and P. Adamova (2014). Reassessment of the rifting process in the western Corinth rift from relocated seismicity, *Geophys. J. Int.* **197,** 1822–1844, doi: 10.1093/gji/ggu096.

Makropoulos, K., G. Kaviris, and V. Kouskouna (2012). An updated and extended earthquake catalogue for Greece and adjacent areas since 1900, *Nat. Hazards Earth Syst. Sci.* **12,** 1425–1430, doi: 10.5194/nhess-12-1425-2012.

Mesimeri, M., V. Karakostas, E. Papadimitriou, D. Schaff, and G. Tsaklidis (2016). Spatio-temporal properties and evolution of the 2013 Aigion earthquake swarm (Corinth Gulf, Greece), *J. Seismol.* **20,** no. 2, 595–614, doi: 10.1007/s10950-015-9546-4.

Rigo, A., H. Lyon-Caen, R. Armijo, A. Deschamps, D. Hatzfeld, K. Makropoulos, P. Papadimitriou, and I. Kassaras (1996). A microseismic study in the western part of the Gulf of Corinth (Greece) implication for large-scale normal faulting mechanisms, *Geophys. J. Int.* **126,** 663–688, doi: 10.1111/j.1365-246X.1996.tb04697.x.

Sakellariou, D., and K. Tsampouraki-Kraounaki (2019). Plio-quaternary extension and strike-slip tectonics in the Aegean, in *Transform Plate Boundaries and Fracture Zones*, J. C. Duarte (Editor), Elsevier, 339–374, doi: 10.1016/B978-0-12-812064-4.00014-1.

Serpetsidaki, A., P. Elias, M. Ilieva, P. Bernard, P. Briole, A. Deschamps, S. Lambotte, H. Lyon-Caen, E. Sokos, and G.-A. Tselentis (2014). New constraints from seismology and geodesy on the $M_w = 6.4$ 2008 Movri (Greece) earthquake: Evidence for a growing strike-slip fault system, *Geophys. J. Int.* **198,** 1373–1386, doi: 10.1093/gji/ggu212.

Serpetsidaki, A., E. Sokos, and G.-A. Tselentis (2016). A ten year Moment Tensor database for western Greece, *Phys. Chem. Earth* **95,** 2–9, doi: 10.1016/j.pce.2016.04.007.

Sokos, E., and J. Zahradnik (2008). ISOLA a Fortran code and a Matlab GUI to perform multiple-point source inversion of seismic data, *Comput. Geosci.* **34,** 967–977, doi: 10.1016/j.cageo.2007.07.005.

Sokos, E., J. Zahradník, A. Kiratzi, J. Janský, F. Gallovič, O. Novotny, J. Kostelecký, A. Serpetsidaki, and G.-A. Tselentis (2012). The January 2010 Efpalio earthquake sequence in the western Corinth Gulf (Greece), *Tectonophysics* **530/531,** 299–309, doi: 10.1016/j.tecto.2012.01.005.

Valkaniotis, S., and S. Pavlides (2016). Late Quaternary and Holocene faults of the northern Gulf of Corinth rift, central Greece, *Bull. Geol. Soc. Greece* **50,** 164, doi: 10.12681/bgsg.11715.

Wessel, P., and W. H. F. Smith (1998). New, improved version of generic mapping tools released, *Eos Trans. AGU* **79,** no. 47, 579 doi: 10.1029/98EO00426.

Zahradník, J., and E. Sokos (2018). ISOLA code for multiple-point source modeling—Review, in *Moment Tensor Solutions Sebastian*, S. D'Amico (Editor), Springer, Cham, Switzerland, 1–28, doi: 10.1007/978-3-319-77359-9_1.

Authors and Affiliations

George Kaviris: Section of Geophysics–Geothermics, Department of Geology and Geoenvironment, National and Kapodistrian University of Athens, Athens, Greece, https://orcid.org/0000-0001-8956-4299; **Panagiotis Elias:** National Observatory of Athens, Institute for Astronomy, Astrophysics, Space Applications and Remote Sensing, Athens, Greece, https://orcid.org/0000-0002-8650-0895; **Vasilis Kapetanidis:** Section of Geophysics–Geothermics, Department of Geology and Geoenvironment, National and Kapodistrian University of Athens, Athens, Greece, https://orcid.org/0000-0002-7811-1216; **Anna Serpetsidaki:** Department of Geology, Seismological Laboratory, University of Patras, Patras, Greece, https://orcid.org/0000-0002-7085-8147; **Andreas Karakonstantis:** Section of Geophysics–Geothermics, Department of Geology and Geoenvironment, National and Kapodistrian University of Athens, Athens, Greece, https://orcid.org/0000-0002-7423-2600; **Vladimír Plicka:** Faculty of Mathematics and Physics, Charles University, Prague, Czech Republic, https://orcid.org/0000-0002-3316-8825; **Louis De Barros:** Observatoire de la Côte d'Azur, Université Côte d'Azur, CNRS, IRD, Géoazur, Nice, France, https://orcid.org/0000-0002-5541-9162; **Efthimios Sokos:** Department of Geology, Seismological Laboratory, University of Patras, Patras, Greece, https://orcid.org/0000-0002-7742-7251; **Ioannis Kassaras:** Section of Geophysics–Geothermics, Department of Geology and Geoenvironment, National and Kapodistrian University of Athens, Athens, Greece, https://orcid.org/0000-0003-1185-9067; **Vassilis Sakkas:** Section of Geophysics–Geothermics, Department of Geology and Geoenvironment, National and Kapodistrian University of Athens, Athens, Greece, https://orcid.org/0000-0002-2466-7446; **Ioannis Spingos:** Section of Geophysics–Geothermics, Department of Geology and Geoenvironment, National and Kapodistrian University of Athens, Athens, Greece, https://orcid.org/0000-0002-5850-5736; **Sophie Lambotte:** EOST, ITES, Université de Strasbourg, CNRS, Strasbourg, France, https://orcid.org/0000-0003-1078-3419; **Clara Duverger:** Commissariat à l'énergie atomique et aux énergies alternatives, DAM, DIF, Paris, France, https://orcid.org/0000-0002-7814-1546; **Olivier Lengliné:** EOST, ITES, Université de Strasbourg, CNRS, Strasbourg, France, https://orcid.org/0000-0003-0678-2587; **Christos P. Evangelidis:** National Observatory of Athens, Institute of Geodynamics, Athens, Greece, https://orcid.org/0000-0001-8733-8984; **Ioannis Fountoulakis:** National Observatory of Athens, Institute of Geodynamics, Athens, Greece, https://orcid.org/0000-0003-1636-133X; **Olga-Joan Ktenidou:** National Observatory of Athens, Institute of Geodynamics, Athens, Greece, https://orcid.org/0000-0001-5206-5699; **František Gallovič:** Faculty of Mathematics and Physics, Charles University, Prague, Czech Republic, https://orcid.org/0000-0002-9268-3923; **Simon Bufféral:** Laboratoire de Géologie, CNRS, École Normale Supérieure, PSL University, Paris, France, https://orcid.org/0000-0002-7360-0854; **Emilie Klein:** Laboratoire de Géologie, CNRS, École Normale Supérieure, PSL University, Paris, France, https://orcid.org/0000-0003-3239-5118; **El Madani Aissaoui:** Équipe de Sismologie, Institut de Physique du Globe de Paris, Paris, France, https://orcid.org/0000-0003-1435-0936; **Oona Scotti:** Bureau d'Évaluation des Risques Sismiques pour la Sûreté des Installations, IRSN, Fontenay-aux-Roses, France, https://orcid.org/0000-0002-6640-9090; **Helene Lyon-Caen:** Laboratoire de Géologie, CNRS, École Normale Supérieure, PSL University, Paris, France, https://orcid.org/0000-0002-6331-0108; **Alexis Rigo:** Laboratoire de Géologie, CNRS, École Normale Supérieure, PSL University, Paris, France, https://orcid.org/0000-0002-5958-9839; **Panayotis Papadimitriou:** Section of Geophysics–Geothermics, Department of Geology and Geoenvironment, National and Kapodistrian University of Athens, Athens, Greece; **Nicholas Voulgaris:** Section of Geophysics–Geothermics, Department of Geology and Geoenvironment, National and

Kapodistrian University of Athens, Athens, Greece, https://orcid.org/0000-0001-6551-1360; **Jiri Zahradnik:** Faculty of Mathematics and Physics, Charles University, Prague, Czech Republic, https://orcid.org/0000-0002-1307-2957; **Anne Deschamps:** Observatoire de la Côte d'Azur, Université Côte d'Azur, CNRS, IRD, Géoazur, Nice, France, https://orcid.org/0000-0002-6209-9814; **Pierre Briole:** Laboratoire de Géologie, CNRS, École Normale Supérieure, PSL University, Paris, France, https://orcid.org/0000-0001-6805-6295; and **Pascal Bernard:** Équipe de Sismologie, Institut de Physique du Globe de Paris, Paris, France

Manuscript received 9 June 2021
Published online 20 July 2021